

An Input-Output Data-Driven Dissipativity Approach for Compositional Stability Certification of Interconnected LTI MIMO Systems

Alejandra Sandoval-Carranza * Juan E. Machado *
 Johannes Schiffer **

* Brandenburg University of Technology Cottbus-Senftenberg, 03046 Cottbus, Germany (e-mail: {sandoval, machadom, schiffer}@b-tu.de).

** Fraunhofer IEG, Fraunhofer Research Institution for Energy Infrastructures and Geotechnologies IEG, 03046 Cottbus, Germany (e-mail: johannes.schiffer@ieg.fraunhofer.de).

Abstract: We propose an input-output data-driven framework for certifying the stability of interconnected multiple-input-multiple-output linear time-invariant discrete-time systems via QSR-dissipativity. That is, by using measured input-output trajectories of each subsystem, we verify dissipative properties and extract local passivity indices without requiring an explicit model identification. These passivity indices are then used to derive conditions under which the equilibrium of the interconnected system is stable. In particular, the framework identifies how the lack of passivity in some subsystems can be compensated by surpluses in others. The proposed approach enables a compositional stability analysis by combining subsystem-level conditions into a criterion valid for the overall interconnected system. We illustrate via a numerical case study, how to compute channel-wise passivity indices and infer stability guarantees directly from data with the proposed method.

Keywords: Dissipativity; Data-driven control; Interconnected systems; Compositional stability analysis.

1. INTRODUCTION

1.1 Motivation

In many modern infrastructures—such as power systems, transportation and communication networks—there exist complex interdependencies that can compromise overall stability and reliable operation: in power systems, the rapid integration of renewable and distributed resources intensifies dynamic couplings and reduces inertia, fundamentally challenging traditional notions of stability (Laib et al., 2023; Cucuzzella et al., 2024; Machado et al., 2023; Schiffer et al., 2016, 2019); in formation control of mobile robots, changes in the communication or sensing graph can cause formation errors or instability (Fax and Murray, 2004). Similar challenges appear across multi-agent and networked control systems more broadly, where heterogeneity, subsystem coupling, and limited measurements complicate stability assessment (Weiland and Cheng, 2022; Hill and Liu, 2022). In such settings, compositional criteria are more beneficial and easier to apply than centralized ones (Martinelli et al., 2024; Arcak, 2022). Moreover, there is an emerging interest in moving from traditional model-based analysis to data-driven concepts due to the growing ease of obtaining and processing data as well as the increase in system complexity (De Persis and Tesi, 2019; van Waarde et al., 2023).

1.2 Literature Review

Existing stability assessment frameworks for interconnected systems are typically model-based (Machado and Schiffer, 2020; Martinelli et al., 2024) and assume diffusive (e.g., Laplacian-type) interconnection structures (Malan et al., 2025;

Martinelli et al., 2024). Within the available literature, dissipativity and passivity theories provide a rigorous foundation for compositional analysis by quantifying energy exchange between a subsystem and the environment in which it is embedded (Willems, 1972; Lozano et al., 2013). In particular, passivity indices, which can quantify a system's deviation from passivity (Khalil and Grizzle, 2002), have enabled the provision of decentralized stability guarantees and guided controller design in networked settings (He and Dörfler, 2024; Malan et al., 2024). However, both dissipativity and passivity assessment approaches conventionally rely on explicit system models, limiting their applicability in large-scale or uncertain settings, see Machado and Schiffer (2020); Strehle et al. (2024); Martinelli et al. (2024).

To address this issue, more recently data-based approaches have been proposed for verifying dissipativity properties directly from measured system trajectories, see van Waarde et al. (2022); Koch et al. (2022); Van Waarde et al. (2023); Markovsky and Dörfler (2021). Most of the available solutions that can be tailored for the analysis and control of MIMO systems are input-state approaches, i.e., they rely on full-state measurements, see De Persis and Tesi (2019); van Waarde et al. (2023); Nakano et al. (2025). However, in many applications obtaining full state measurements is infeasible, especially in large-scale systems. Therefore, data-driven input-output methods that allow for dissipativity assessment based solely on input and output trajectories are more appealing. Yet, existing methods are limited in the sense that formulations assume zero initial conditions (Maupong et al., 2017; Rosa and Jayawardhana, 2021), focus on SISO settings (Koch et al., 2022; De Persis and Tesi, 2019), and their application to MIMO interconnected

systems remains limited (Alsatti et al., 2025; Verhoek et al., 2024).

1.3 Contributions

In light of the above discussion, the main contributions of this work are summarized as follows:

- By using an input-output data-driven approach, we report an LMI-based characterization of QSR-dissipativity for discrete-time LTI MIMO systems, without resorting to stringent assumptions on the systems initial conditions.
- By introducing the notion of *channel-wise* passivity indices, we exploit the proposed data-based QSR-dissipativity assessment approach for deriving a flexible compositional criterion for investigating the stability of interconnected LTI MIMO systems based solely on local input-output data, i.e., without relying on centrally available system data or measurements.
- Via a case study based on a realistically parameterized DC microgrid model, we illustrate the applicability and interpretability of the proposed data-based compositional stability criterion, allowing us to visualize the effect of faults in energy generation units on the channel-wise passivity indices and the overall system stability.

1.4 Paper Organization

The article is organized as follows. In Section II, we provide the necessary preliminaries and notation. In Section III, we state the problem and describe the considered system interconnection structure. In Section IV, we develop the compositional stability analysis based on QSR-dissipativity and channel-wise passivity indices. In Section V, we illustrate the results on a numerical DC microgrid example. In Section VI, we conclude the paper.

1.5 Notation

We denote the set of integer numbers by \mathbb{Z} and the set of real numbers by \mathbb{R} . For a signal $z : \mathbb{Z} \rightarrow \mathbb{R}^n$ and two integers i and k , with $i \leq k$, we employ the notation $z_{[i,k]} := \{z(i), z(i+1), \dots, z(k)\}$. For a signal z and a positive integer T , we follow De Persis and Tesi (2019) and define the Hankel matrix associated to z as:

$$Z_{\{i,T\}} = \begin{bmatrix} z(i) & \cdots & z(i+T-1) \\ \vdots & \ddots & \vdots \\ z(i+T-1) & \cdots & z(i+T-2) \end{bmatrix} \in \mathbb{R}^{tn \times T}, \quad (1)$$

where the subscript i denotes the time at which the first sample of the signal is taken, tn the number of rows and T the number of columns. When $t = 1$, we denote (De Persis and Tesi, 2019):

$$Z_{\{i,T\}} := [z(i) \ z(i+1) \ \cdots \ z(T+i-1)] \in \mathbb{R}^{n \times T}. \quad (2)$$

For a matrix $A \in \mathbb{R}^{n \times m}$, A^\dagger denotes its Moore-Penrose inverse.

2. PRELIMINARIES

In this section, we introduce instrumental concepts and results about QSR-dissipative systems and data-based characterization of discrete-time linear time-invariant (LTI) multiple-input-multiple-output (MIMO) systems.

2.1 QSR-Dissipativity

We consider the following discrete-time LTI MIMO system:

$$\begin{aligned} x(k+1) &= Ax(k) + Bu(k), \\ y(k) &= Cx(k), \end{aligned} \quad (3)$$

where $x \in \mathbb{R}^n$, $u \in \mathbb{R}^m$, and $y \in \mathbb{R}^p$ are the state, input and output vector, respectively. A standing technical assumption throughout this section is that the system (3) is controllable and observable.

We employ the following standard notions of dissipativity and QSR-dissipativity (Byrnes and Lin, 1994; Martinelli et al., 2024).

Definition 2.1. (Dissipativity). The system (3) is said to be *dissipative* with respect to the supply rate $w : \mathbb{R}^m \times \mathbb{R}^p \rightarrow \mathbb{R}$ if there exists a nonnegative function $V : \mathbb{R}^n \rightarrow \mathbb{R}$, called a storage function, such that for all $u \in \mathbb{R}^m$, all $k \in \mathbb{N}$ and any initial condition $x(0) \in \mathbb{R}^n$,

$$V(x(k+1)) - V(x(k)) \leq w(u(k), y(k)). \quad (4)$$

Definition 2.2. (QSR-dissipativity). The system (3) is said to be *QSR-dissipative* if it is dissipative with respect to the supply rate

$$w(u(k), y(k)) = \begin{bmatrix} y(k) \\ u(k) \end{bmatrix}^\top \begin{bmatrix} Q & S \\ S^\top & R \end{bmatrix} \begin{bmatrix} y(k) \\ u(k) \end{bmatrix}, \quad (5)$$

where $Q = Q^\top \in \mathbb{R}^{p \times p}$, $S \in \mathbb{R}^{p \times m}$ and $R = R^\top \in \mathbb{R}^{m \times m}$.

An LMI-based necessary and sufficient condition for QSR-dissipativity is as follows (Moylan and Hill, 1978; Koch et al., 2022).

Theorem 1. The system (3) is QSR-dissipative with storage function $V(x(k)) = x(k)^\top Px(k)$ if and only if there exists a matrix $P = P^\top \geq 0$, such that

$$\begin{bmatrix} A^\top PA - P - C^\top QC & A^\top PB - C^\top S \\ (A^\top PB - C^\top S)^\top & B^\top PB - R \end{bmatrix} \leq 0. \quad (6)$$

Now we introduce the concept of passivity indices, which are associated to a specific form of QSR-dissipativity and, depending on sign conditions, quantify the deviations from passivity and variants of it, see (Khalil and Grizzle, 2002, Ch. 6) and (Lozano et al., 2013, Ch. 2).

Definition 2.3. (Passivity indices). The system (3) with $m = p$ has *passivity indices* $(\rho, v) \in \mathbb{R}^2$ when the supply rate in (5) is chosen as

$$Q = -\rho I_m, \quad S = \frac{1}{2} I_m, \quad R = -v I_m. \quad (7)$$

If $\rho > 0$ ($v > 0$), the system exhibits an *excess of output (input) passivity*; conversely, if $\rho < 0$ ($v < 0$), it shows a *shortage of output (input) passivity*.

In MIMO systems, different input-output channels may contribute unevenly to the energy exchange with the environment. Then, having scalar global indices ρ and v may bring undesired conservativeness, particularly when analyzing the interconnection with other systems. The establishment of one of our main contributions relies on the slightly more general notion of input-output *channel-wise* passivity indices $(\rho_1, \dots, \rho_m, v_1, \dots, v_m)$, which originates from the system (3) being QSR-dissipative with

$$Q = - \begin{bmatrix} \rho_1 & \cdots & 0 \\ \vdots & \ddots & \vdots \\ 0 & \cdots & \rho_m \end{bmatrix}, \quad S = \frac{1}{2} I_m, \quad R = - \begin{bmatrix} v_1 & \cdots & 0 \\ \vdots & \ddots & \vdots \\ 0 & \cdots & v_m \end{bmatrix}, \quad (8)$$

for some real numbers $\rho_i \in \mathbb{R}$, $v_i \in \mathbb{R}$, $i = 1, 2, \dots, m$.

The solvability of (6) hinges upon the precise knowledge of the coefficient matrices A , B and C . In the following subsection, inspired by Alsalti et al. (2025); Koch et al. (2022), we present a data-based condition that only requires measured input–output data.

2.2 Data-Based Dissipativity Characterization of MIMO LTI Systems

Consider once again (3) and henceforth assume that A , B and C are unknown. Let $u_{[0,T]}$ and $y_{[0,T]}$ denote measured input and output trajectories over a discrete-time horizon $T \in \mathbb{N}$, respectively. To assess whether (3) is QSR-dissipative, we follow Alsalti et al. (2025) to characterize a minimal realization of (3) directly from the measured input–output data.

Let ℓ denote the lag of (3), which is defined as the smallest integer such that $\text{rank}(O_\ell) = n$, where

$$O_\ell = \left[C^\top \ (CA)^\top \ \dots \ (CA^{\ell-1})^\top \right]^\top \in \mathbb{R}^{p\ell \times n}.$$

Assume that $\ell \leq n \leq p\ell$ (Alsalti et al., 2025) (see also Willems (1986)). We also require the following standard condition on the input signal (Willems et al., 2005).

Definition 2.4. (Persistency of excitation). The input sequence $u_{[0,T]}$ is *persistently exciting* of order $\ell + n + 1$ if the Hankel matrix constructed from $u_{[0,T]}$ has full row rank.

Then, in accordance to (Alsalti et al., 2025, Lemma 1), if $u_{[0,T]}$ is persistently exciting, then

$$\text{rank} \left(\begin{bmatrix} U_{\{-\ell, \ell+1, T-1\}} \\ Y_{\{-\ell, \ell, T-2\}} \end{bmatrix} \right) = m(\ell + 1) + n. \quad (9)$$

Here, $U_{\{-\ell, \ell+1, T-1\}}$ and $Y_{\{-\ell, \ell, T-2\}}$ denote the Hankel matrices constructed from the input and output trajectories $u_{[0,T]}$ and $y_{[0,T]}$, respectively, following the notation introduced in Section 2.1.

Now let $z(k) \in \mathbb{R}^{m\ell+n}$ be a vector defined in terms of the measured data as follows:

$$z(k) = \begin{bmatrix} u_{[k-\ell, k-1]} \\ \overline{\Theta} y_{[k-\ell, k-1]} \end{bmatrix}, \quad (10)$$

where $\overline{\Theta} \in \mathbb{R}^{n \times p\ell}$ is obtained by selecting n linearly independent rows of $Y_{\{-\ell, \ell, T-2\}}$. This can always be done due to (9) and the fact that $u_{[0,T]}$ is persistently exciting of order $\ell + n + 1$ and thus $\text{rank}(U_{\{-\ell, \ell+1, T-1\}}) = m(\ell + 1)$. In Alsalti et al. (2025) it has been shown that $z(k)$ is a non-minimal state vector for (3), i.e., there exists a full row rank matrix $\hat{T} \in \mathbb{R}^{n \times (m\ell+n)}$, such that $x(k) = \hat{T}z(k)$ for all $k \in \mathbb{Z}$. Then, there exist (unknown) matrices \mathcal{A} , \mathcal{B} and \mathcal{C} , such that

$$\begin{aligned} z(k+1) &= \mathcal{A}z(k) + \mathcal{B}u(k), \\ y(k) &= \mathcal{C}z(k). \end{aligned} \quad (11)$$

The system (11) has the same input–output behavior as (3). We present next how, subject to (9), it is possible to produce directly from $u_{[0,T]}$ and $y_{[0,T]}$ an equivalent data-based representation of (11):

Consider the system (11) and the original input sequence $u_{[0,T]}$. By computing the trajectory sequence $z_{[0,T]}$ in (10) and recalling the notation introduced in (2), it is then possible to define the following (input–state) Hankel matrix associated to (11):

$$H(u, z) = \begin{bmatrix} U_{\{0, T-1\}} \\ Z_{\{0, T-1\}} \end{bmatrix} \in \mathbb{R}^{(m(\ell+1)+n) \times T}. \quad (12)$$

In Alsalti et al. (2025), by establishing a linear relationship between $H(u, z)$ and the (input–output) Hankel matrix on the left-hand side of (9), it was shown that $\text{rank}(H(u, z)) = m(\ell + 1) + n$. Therefore, it is possible to state the following result.

Lemma 2.1. Assume that $u_{[0,T]}$ is persistently exciting of order $\ell + n + 1$. Then, the non-minimal representation (11) has the following equivalent data-based representation:

$$\begin{aligned} z(k+1) &= Z_{\{1, T\}} \begin{bmatrix} U_{\{0, T-1\}} \\ Z_{\{0, T-1\}} \end{bmatrix}^\dagger \begin{bmatrix} u(k) \\ z(k) \end{bmatrix}, \\ y(k) &= Y_{\{0, T-1\}} Z_{\{0, T-1\}}^\dagger z(k), \end{aligned} \quad (13)$$

where, $U_{\{0, T-1\}}$ and $Y_{\{0, T-1\}}$ follow the Hankel notation used in (9), while $Z_{\{0, T-1\}}$ is the corresponding Hankel matrix constructed from the trajectory $z_{[0,T]}$ as in (12).

Proof. The proof can be established following a procedure analogous to the one used in (De Persis and Tesi, 2019, Theorem 1) and is omitted due to space constraints.

Moving forward, we can obtain the coefficient matrices \mathcal{A} , \mathcal{B} and \mathcal{C} that define (11) as follows (c.f., Koch et al. (2022)):

$$\begin{aligned} \mathcal{A} &= \text{Proj}_{m+1:(m+p)n+m} (Z_{\{1, T\}} H(u, z)^\dagger), \\ \mathcal{B} &= \text{Proj}_{1:m} (Z_{\{1, T\}} H(u, z)^\dagger), \\ \mathcal{C} &= Y_{\{0, T-1\}} Z_{\{0, T-1\}}^\dagger, \end{aligned} \quad (14)$$

where $\text{Proj}_{a:b}(\cdot)$ denotes the selection of rows a to b from the given matrix. Using Kalman decomposition (Chen, 1984, Theorem 6.7), it is possible to use (14) to construct a minimal state-space realization which is *equivalent* to (3). Let \hat{A}_i , \hat{B}_i , and \hat{C}_i denote the corresponding minimal realization system matrices, defined as

$$\hat{A}_i = T_{\text{co},i}^\top \mathcal{A}_i T_{\text{co},i}, \quad \hat{B}_i = T_{\text{co},i}^\top \mathcal{B}_i, \quad \hat{C}_i = \mathcal{C}_i T_{\text{co},i}, \quad (15)$$

where $(\mathcal{A}_i, \mathcal{B}_i, \mathcal{C}_i)$ are defined as in (14), and $T_{\text{co},i}$ is an orthogonal matrix whose columns span the controllable and observable subspace¹. Then, we have the following result.

Theorem 2. Assume that $u_{[0,T]}$ is persistently exciting of order $\ell + n + 1$ and consider the matrices introduced in (14). Then, (3) is QSR-dissipative if and only if there exists a matrix $\hat{P} = \hat{P}^\top \geq 0$, such that

$$\begin{bmatrix} \hat{A}^\top \hat{P} \hat{A} - \hat{P} - \hat{C}^\top Q \hat{C} & \hat{A}^\top \hat{P} \hat{B} - \hat{C}^\top S \\ (\hat{A}^\top \hat{P} \hat{B} - \hat{C}^\top S)^\top & \hat{B}^\top \hat{P} \hat{B} - R \end{bmatrix} \leq 0, \quad (16)$$

where Q , S and R are as in (8).

Proof. The proof is a direct application of Theorem 1 after noting that (16) implies QSR-dissipativity of the minimal system realization $\hat{x}(k+1) = \hat{A}\hat{x}(k) + \hat{B}u$, $y = \hat{C}\hat{x}$, which is equivalent to (3).

3. PROBLEM STATEMENT AND MAIN RESULT

Having established the necessary background in the previous section, we are in position to formulate the problem statement and present our main result.

¹ The controllable and observable subspace of a state-space triple (A, B, C) is defined as $\mathcal{R} \cap \mathcal{U}^\perp$, where \mathcal{R} is the column space of the controllability matrix and \mathcal{U} is the kernel of the observability matrix (Chen, 1984).

3.1 Problem Statement

Consider a network of $N > 1$ interconnected subsystems Σ_i , whose dynamics are discrete-time LTI MIMO of the form:

$$\Sigma_i : \begin{aligned} x_i(k+1) &= A_i x_i(k) + B_i u_i(k), \\ y_i(k) &= C_i x_i(k), \end{aligned} \quad (17)$$

where $x_i(k) \in \mathbb{R}^{n_i}$, $u_i(k) \in \mathbb{R}^{m_i}$ and $y_i(k) \in \mathbb{R}^{m_i}$. We assume that the matrices A_i , B_i , and C_i are unknown, and that each subsystem Σ_i is controllable and observable. Moreover, let $M_i = \{1, 2, \dots, m_i\}$ be the index set of input-output pairs for the i -th subsystem. For each $j \in M_i$, we assume that there exists a unique pair (a, b) , with

$$a \in \{1, 2, \dots, N\} \setminus \{i\}, \quad b \in M_a, \quad (18)$$

such that the interaction among the two subsystems i and a is carried out through the following feedback interconnection law of their j -th and b -th channel:

$$u_{i,j} = y_{a,b}, \quad u_{a,b} = -y_{i,j}. \quad (19)$$

Then, the main problem we address in this paper is as follows: Assuming that input-output measurement sets, $u_{[0, T_i]}$ and $y_{[0, T_i]}$, are locally available to its corresponding subsystem Σ_i , derive data-based and tractable compositional conditions to assess whether the overall interconnected system (17), (19), $i = 1, \dots, N$, is stable.

3.2 Main Result

As our main result, we present compositional data-based conditions for certifying the stability of interconnected discrete time LTI MIMO systems, subject to the availability of sufficiently rich local input-output data. Conditions for asymptotic stability are given in Corollary 3.1.

Theorem 3. Consider the interconnected system (17), (19), $i = 1, \dots, N$. For each subsystem Σ_i assume that input-output data sequences $u_{[0, T_i]}$ and $y_{[0, T_i]}$ are available to each subsystem, where $u_{[0, T_i]}$ is persistently exciting of order $\ell_i + n_i + 1$. Then, the origin of the interconnected system is stable if there exist matrices $\hat{P}_i = \hat{P}_i^\top > 0$, such that

$$\begin{bmatrix} \hat{A}_i^\top \hat{P}_i \hat{A}_i - \hat{P}_i - \hat{C}_i^\top Q_i \hat{C}_i & \hat{A}_i^\top \hat{P}_i \hat{B}_i - \hat{C}_i^\top S_i \\ (\hat{A}_i^\top \hat{P}_i \hat{B}_i - \hat{C}_i^\top S_i)^\top & \hat{B}_i^\top \hat{P}_i \hat{B}_i - R_i \end{bmatrix} \leq 0, \quad (20a)$$

$$\begin{bmatrix} -\rho_{i,j} - v_{a,b} & 0 \\ 0 & -\rho_{a,b} - v_{i,j} \end{bmatrix} \leq 0, \quad (20b)$$

where

$$\begin{aligned} Q_i &= \text{diag}(-\rho_{i,1}, -\rho_{i,2}, \dots, -\rho_{i,m_i}), \\ R_i &= \text{diag}(-v_{i,1}, -v_{i,2}, \dots, -v_{i,m_i}), \\ S_i &= \frac{1}{2} I_{m_i \times m_i}, \end{aligned} \quad (21)$$

where $(\hat{A}_i, \hat{B}_i, \hat{C}_i)$ is given in (15).

Proof. By Theorem 2 the existence of $\hat{P}_i > 0$ satisfying (20a) implies that each subsystem Σ_i is QSR-dissipative with positive-definite quadratic storage function $V_i(x_i(k)) = \frac{1}{2} x_i^\top(k) P x_i(k)$ and with respect to the supply rate

$$w_i(u_i(k), y_i(k)) = \begin{bmatrix} y_i(k) \\ u_i(k) \end{bmatrix}^\top \begin{bmatrix} Q_i & S_i \\ S_i^\top & R_i \end{bmatrix} \begin{bmatrix} y_i(k) \\ u_i(k) \end{bmatrix}. \quad (22)$$

Let $V(x(k)) = \sum_{i=1}^N V_i(x_i(k))$ be a candidate Lyapunov function for showing that the origin of the interconnected system (17),

(19), $i = 1, \dots, N$, is stable. Then, due to QSR-dissipativity of each Σ_i it holds that

$$V(x(k+1)) - V(x(k)) \leq \sum_{i=1}^N w_i(u_i(k), y_i(k)). \quad (23)$$

We write now an equivalent expression for the right-hand side of (23). Considering the structures for Q_i , S_i and R_i in (21), we obtain from (5) that

$$\sum_{i=1}^N w_i(u_i(k), y_i(k)) = \sum_{i=1}^N \sum_{j \in M_i} (-\rho_{i,j} y_{i,j}^2 + y_{i,j} u_{i,j} - v_{i,j} u_{i,j}^2), \quad (24)$$

where we recall that $M_i = \{1, 2, \dots, m_i\}$ is the index set of input-output pairs in subsystem Σ_i . Now, due to the interconnection law (19), it holds that each term $(y_{i,j}, u_{i,j})$ has a *unique* counterpart $(y_{a,b}, u_{a,b})$, such that the corresponding two elements in (24) are given by

$$\begin{aligned} &-\rho_{i,j} y_{i,j}^2 + y_{i,j} y_{a,b} - v_{a,b} y_{i,j}^2 - \rho_{a,b} y_{a,b}^2 - y_{a,b} y_{i,j} - v_{i,j} y_{a,b}^2 \\ &= -(\rho_{i,j} + v_{a,b}) y_{i,j}^2 - (\rho_{a,b} + v_{i,j}) y_{a,b}^2. \end{aligned}$$

Let Π_i be the set of all pairs (a, b) such that the channels (i, j) and (a, b) are interconnected according to (19). For each subsystem $k \neq i$, we define

$$\mathcal{K}_{k,i} := \{j \in M_i \mid \exists b \in M_k \text{ such that } (k, b) \in \Pi_i\}. \quad (25)$$

This set collects the input-output channels of Σ_i that are interconnected with subsystem Σ_k . Therefore, the following identities can be obtained:

$$\begin{aligned} \sum_{i=1}^N w_i(u_i(k), y_i(k)) &= \\ \sum_{i=1}^N \sum_{j \in M_i} &(-\rho_{i,j} y_{i,j}^2 + y_{i,j} u_{i,j} - v_{i,j} u_{i,j}^2) = \\ \sum_{i=1}^{N-1} \sum_{j \in M_i \setminus \bigcup_{k=1}^{i-1} \mathcal{K}_{k,i}} &\begin{bmatrix} y_{i,j} \\ y_{a,b} \end{bmatrix}^\top \begin{bmatrix} -\rho_{i,j} - v_{a,b} & 0 \\ 0 & -\rho_{a,b} - v_{i,j} \end{bmatrix} \begin{bmatrix} y_{i,j} \\ y_{a,b} \end{bmatrix}. \end{aligned} \quad (26)$$

The union $\bigcup_{k=1}^{i-1} \mathcal{K}_{k,i}$ ensures that each interconnection pair is counted only once. In view of (20b) and (23), we obtain that

$$V(x(k+1)) - V(x(k)) \leq 0, \quad (27)$$

which implies that V is a Lyapunov function for the origin of the interconnected system and, consequently, the origin is stable.

The next two corollaries follow from Theorem 3.

Corollary 3.1. Consider the interconnected system (17), (19), $i = 1, \dots, N$. Assume that (20b) holds with strict inequality. Then, the origin of the overall interconnected system is asymptotically stable provided that every subsystem Σ_i is either zero state observable or zero state detectable.

Proof. From Theorem 3, any α -sublevel set Ω_α of the Lyapunov function $V = \sum_{i=1}^N \frac{1}{2} x_i^\top(k) P x_i(k)$ is invariant (with $\alpha > 0$ arbitrary). Moreover, (23) and (26) hold.

Since (20b) holds strictly, it follows that $V(x(k+1)) - V(x(k)) = 0$ if and only if $y_{i,j} = 0$ for every $i = 1, \dots, N$ and every $j \in M_i$. To make this explicit, define the set $\mathcal{E} := \{(x_1, \dots, x_N) : y_{i,j} = 0 \ \forall i, j \in M_i\}$, which characterizes the states for which V remains constant. If each Σ_i is zero-state observable, i.e., $y_{i,j} = 0$ for all i, j implies $x_i = 0$, then V becomes a strict Lyapunov function. In this case, $\mathcal{E} = \{0\}$. Alternatively, if each Σ_i is zero-state detectable, i.e., $y_{i,j} = 0$ for all i, j implies $x_i \rightarrow 0$, then the origin becomes the largest attractive invariant

set contained in $\{(x_1, \dots, x_N) \in \Omega_\alpha : y_{i,j} = 0 \forall j \in M_i\}$. Equivalently, the origin is the largest attractive invariant set contained in $\mathcal{E} \cap \Omega_\alpha$. By LaSalle's invariance principle (Mei and Bullo, 2017), for discrete-time systems, the origin is asymptotically stable.

Corollary 3.2. Consider the interconnected system (17), (19). For each subsystem Σ_i , its channel-wise passivity indices $(\rho_{i,j}, v_{i,j})$ can be obtained as the solution of the optimization problem

$$\max_{\rho_{i,j}, v_{i,j}} f(\rho_{i,j}, v_{i,j}), \quad (28)$$

subject to the local QSR-dissipativity condition (20a) and the stability condition (20b) for all relevant pairs involving $(\rho_{i,j}, v_{i,j})$. Moreover, the computation can be carried out in a distributed manner, in the sense that each subsystem enforces (20a) using its own input–output data, while the constraints (20b) only couple indices across directly interconnected subsystems.

Proof.

Both constraints (20a) and (20b) are linear matrix inequalities in $(\hat{P}_i, \rho_{i,j}, v_{i,j})$, and are therefore convex constraints. Hence, if the cost function f in (28) is convex, the optimization problem is convex. Any feasible solution satisfies the imposed dissipativity and stability constraints involving $(\rho_{i,j}, v_{i,j})$ for each subsystem and its neighbors.

4. NUMERICAL EXAMPLE

In this section, for a low-voltage DC microgrid we illustrate the proposed data-based dissipativity analysis. Using measured input–output trajectories of four distinct system areas, we evaluate local QSR-dissipativity properties before and after generation-outage contingencies, and illustrate the associated changes in the channel-wise passivity indices and the implication for the verification of the compositional stability condition introduced in Section III.

4.1 Simulation Setup

The considered microgrid setup shown in Fig. 1 is a variant of the case study reported in Cucuzzella et al. (2019), which consists of four main areas, each with local power generation and consumption, and which are interconnected through resistive-inductive power lines. For reproducibility, the main parameters and configuration used to generate the input–output data are reported in Appendix A, although the data-based analysis does not rely on explicit model knowledge. We consider the following three generation–outage contingencies: at $t = 0$ s the microgrid is initialized at a stable steady-state and remains so until $t = 25$ s, when a single contingency is simulated through the opening sw_i , which implies the disconnection of the generation unit of Area $i = 2, 3, 4$, see Fig. 1.

The data-driven workflow is illustrated using the outage of generation unit $i = 4$ as the baseline scenario. For each scenario, the generation unit is assumed to remain disconnected for the remainder of the simulation². Moreover, the interconnections among the areas obey the following relations, which are consistent with the interconnection law (19):

² For the discrete-time analysis, we use the zero-order hold (zoh) sampled-data realization with period $T_s = 3.4 \times 10^{-4}$ s.

$$\begin{aligned} u_1 &= [-y_{4,2} \ y_{2,1}]^\top, & u_3 &= [-y_{2,2} \ y_{4,1}]^\top, \\ u_2 &= [-y_{1,2} \ y_{3,1}]^\top, & u_4 &= [-y_{3,2} \ y_{1,1}]^\top. \end{aligned} \quad (29)$$

Considering the definition of the coefficient matrices C_i in (A.1) and (A.2), the measured output of each area is given by $y_i = [v_{g,i} \ i_{i,j}]^\top$. For each i , the input $u_i = [u_{i,1} \ u_{i,2}]^\top$ is comprised of the current $u_{i,1}$ of one of the power lines incident to Area i , and the bus voltage $u_{i,2}$ at the other end bus of the line $\{i, j\}$ already embedded in Area i . Thus, the relations in (29) satisfy those in (19).

4.2 Numerical Results

In order to carry out the proposed data-driven analysis, we assume that basic information about the composition of each microgrid area is available: each area is known to have a converter, a local ZI load, an RL line, and a PI controller. Hence, each area has four dynamic components. Consequently, we infer for the input–output data-driven analysis that each area has to be represented by a fourth-order system ($n = 4$) with two input–output pairs. Since we have two measured outputs per area, we set the Hankel lag to $\ell = 2$, satisfying $\ell \leq 4 \leq 2\ell$ (see Section 2.1). After a fault, the disconnected area behaves as a second-order system ($n = 2, \ell = 1$), while other areas remain fourth-order ($n = 4, \ell = 2$).

Figure 2 shows the system evolution from $t = 0$ s to $t = 60$ s for the baseline scenario in which the generation unit of Area 4 is disconnected at $t = 25$ s.

The proposed data-based analysis is independently implemented both on the pre-fault and the post-fault conditions. For both conditions we first verify that the measured input–output data meet the rank condition (9), ensuring persistent excitation of the measured data for the model order n and Hankel lag ℓ . Then, for each area we construct a non-minimal data-based representation (Lemma 2.1), from which we obtain a minimal realization as in (15). The minimal realization models are then used to evaluate the QSR-dissipativity condition in Theorem 2 and compute the channel-wise passivity indices needed for verifying the stability condition in Theorem 3. We note that the interconnection law (19) holds in this example, and we can thus solve a convex optimization problem for computing the channel-wise passivity as outlined in Corollary 3.2: the optimization problem is solved using YALMIP, see Lofberg (2004), and considering the cost function $f(\rho) = \min(-\sum_j \rho_{i,j})$ and a 10^{-3} numerical tolerance on the stability constraints.

The resulting channel-wise passivity indices are summarized in Table 1. Across all areas, every channel exhibits an excess of output passivity (all $\rho_{i,j} > 0$) and a shortage of input passivity (all $v_{i,j} < 0$). In the pre-fault window, Areas 1 and 4 exhibit the largest passivity margins, whereas Areas 2 and 3 show the smallest ones, with $\rho_{2,2}$ and $\rho_{3,1}$ being the lowest entries. After the fault, several channels in Areas 1, 2, and 4 experience reductions, with the most notable decreases in $\rho_{1,1}$ and $\rho_{2,2}$. Although all $\rho_{i,j}$ indices remain positive, the post-fault values indicate a reduced excess of output passivity in the affected areas, while the compositional stability condition of Theorem 3 continues to hold.

We also evaluated pre-fault and post-fault dissipativity for contingencies in Areas 2 and 3, where the corresponding generation unit is disconnected at $t = 25$ s. In these cases, distinct PI

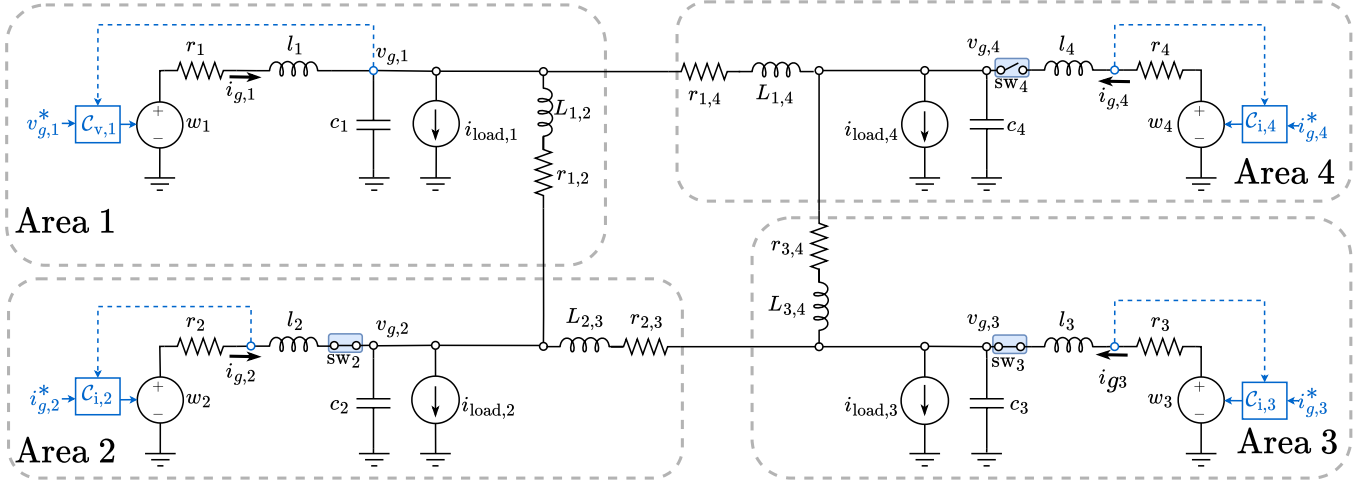


Fig. 1. Low-voltage DC microgrid used in the numerical study. The four areas (gray dashed boxes) are interconnected by the power lines $\{1, 2\}$, $\{2, 3\}$, $\{3, 4\}$, and $\{1, 4\}$ with parameters (r_{ij}, L_{ij}) . In each area, (r_i, l_i) models the converter filter, c_i the local bus capacitor, $v_{g,i}$ the bus voltage, and $i_{\text{load},i}$ the aggregated load. All loads are of ZI type. Area 1 operates in voltage-setting mode (PI controller $C_{v,1}$ regulates $v_{g,1}$ towards a reference), whereas Areas 2–4 operate in current-setting mode (PI controllers regulate $i_{g,i}$ towards a reference). The local switches $sw_i = 2, 3, 4$, can be opened to emulate $N-1$ generation-outage contingencies.

Table 1. Comparison of pre- and post-fault channel-wise passivity indices.

Area	$\rho_{i,1}^{\text{pre}}$	$\rho_{i,1}^{\text{post}}$	$\rho_{i,2}^{\text{pre}}$	$\rho_{i,2}^{\text{post}}$	$v_{i,1}^{\text{pre}}$	$v_{i,1}^{\text{post}}$	$v_{i,2}^{\text{pre}}$	$v_{i,2}^{\text{post}}$
1	0.6004	0.5654	0.6098	0.6366	-1.2000	-1.0460	-0.4421	-0.4388
2	0.4431	0.4398	0.5666	0.5155	-0.6088	-0.6356	-0.4079	-0.4095
3	0.4089	0.4105	0.8618	0.8550	-0.5056	-0.5145	-0.5177	-0.4940
4	0.5187	0.4950	1.2012	1.0470	-0.8608	-0.8540	-0.5994	-0.5644

gains were selected for each scenario and kept fixed throughout the simulation, since other gain choices led to data that either violated the persistency of excitation condition or produced unreliable data-based realizations due to discretization and sampling effects. The parameter sets in Table 2 yield informative trajectories and consistent identified models in both time windows. With these parametrizations, the channel-wise passivity indices display the same qualitative trends as in the baseline case, so that we don't report them here explicitly. Likewise, the post-fault equilibria in all scenarios satisfy the compositional stability condition of Theorem 3.

Table 2. PI control gains for the fault scenarios in Areas 2 and 3.

Scenario		Area 1	Area 2	Area 3	Area 4
sw ₂ open	k_{prop} (-)	1.5	1	11	18
	k_{integ} (s^{-1})	100	1	9	12
sw ₃ open	k_{prop} (-)	1.5	29	1	18
	k_{integ} (s^{-1})	100	28	1	16

5. CONCLUSION AND FUTURE WORK

We have presented a compositional data-driven method for assessing the stability of interconnected MIMO LTI systems based solely on input-output measurement data of each of the component subsystems. Our approach relies on the data-based characterization of non-minimal state-space representations of all the component subsystems. This allows us to formulate structured LMIs for verifying QSR-dissipativity properties of the subsystems and to assess the stability of the interconnected

system in a compositional manner. The effectiveness of our approach was tested on a numerical example of a DC microgrid facing faults.

In future work, we will investigate local stability properties of networks of interconnected nonlinear systems. Moreover, we will explore control gain tuning approaches that can support the verification of persistency of excitation conditions on the measured data. In addition, we will expand our methodology to deal with experimental/field and noise-corrupted measurements.

ACKNOWLEDGEMENTS

This research is supported by the German Federal Government, the Federal Ministry of Research, Technology and Space and the State of Brandenburg within the framework of the joint project EIZ: Energy Innovation Center (project numbers 85056897 and 03SF0693A) with funds from the Structural Development Act (Strukturstärkungsgesetz) for coal-mining regions.

REFERENCES

Alsatti, M., Lopez, V.G., and Müller, M.A. (2025). Notes on data-driven output-feedback control of linear MIMO systems. *IEEE Transactions on Automatic Control*, 1–8. doi: 10.1109/TAC.2025.3553073.

Arcak, M. (2022). Compositional design and verification of large-scale systems using dissipativity theory: Determining stability and performance from subsystem properties and interconnection structures. *IEEE Control Systems Magazine*, 42(2), 51–62. doi:10.1109/MCS.2021.3139721.

Byrnes, C. and Lin, W. (1994). Losslessness, feedback equivalence, and the global stabilization of discrete-time nonlinear systems. *IEEE Transactions on Automatic Control*, 39(1), 83–98. doi:10.1109/9.273341.

Chen, C.T. (1984). *Linear system theory and design*. Saunders college publishing.

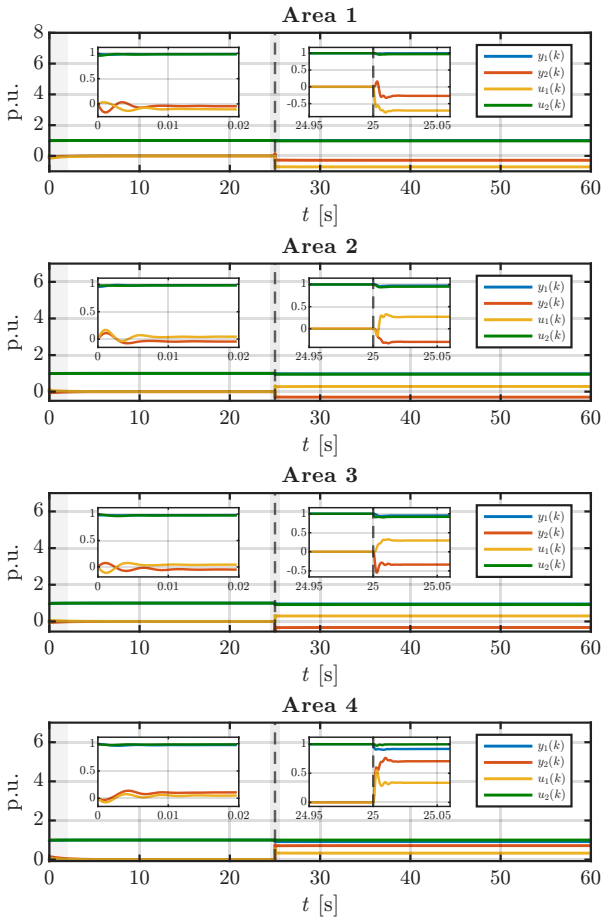


Fig. 2. Pre-fault and Post-fault trajectories of $u_i(t)$ and $y_i(t)$ (p.u.) in Areas 1–4. Insets show zoom over $[0, 0.02]$ s and $[24.95, 25.05]$ s

Cucuzzella, M., Scherpen, J.M., and Machado, J.E. (2024). Microgrids control: AC or DC, that is not the question. In *EPJ Web of Conferences*, volume 310, 00015. EDP Sciences.

Cucuzzella, M., Trip, S., De Persis, C., Cheng, X., Ferrara, A., and van der Schaft, A. (2019). A robust consensus algorithm for current sharing and voltage regulation in DC microgrids. *IEEE Transactions on Control Systems Technology*, 27(4), 1583–1595. doi:10.1109/TCST.2018.2834878.

De Persis, C. and Tesi, P. (2019). Formulas for data-driven control: Stabilization, optimality, and robustness. *IEEE Transactions on Automatic Control*, 65(3), 909–924.

Fax, J. and Murray, R. (2004). Information flow and cooperative control of vehicle formations. *IEEE Transactions on Automatic Control*, 49(9), 1465–1476. doi:10.1109/TAC.2004.834433.

He, X. and Dörfler, F. (2024). Passivity and decentralized stability conditions for grid-forming converters. *IEEE Transactions on Power Systems*, 39(3), 5447–5450. doi:10.1109/TPWRS.2024.3360707.

Hill, D.J. and Liu, T. (2022). Dissipativity, stability, and connections: Progress in complexity. *IEEE Control Systems Magazine*, 42(2), 88–106. doi:10.1109/MCS.2021.3139745.

Khalil, H.K. and Grizzle, J.W. (2002). *Nonlinear systems*, volume 3. Prentice hall Upper Saddle River, NJ.

Koch, A., Berberich, J., and Allgöwer, F. (2022). Provably robust verification of dissipativity properties from data. *IEEE*

Transactions on Automatic Control, 67(8), 4248–4255. doi:10.1109/TAC.2021.3116179.

Laib, K., Watson, J., Ojo, Y., and Lestas, I. (2023). Decentralized stability conditions for DC microgrids: Beyond passivity approaches. *Automatica*, 149, 110705.

Lofberg, J. (2004). YALMIP : a toolbox for modeling and optimization in MATLAB. In *2004 IEEE International Conference on Robotics and Automation (IEEE Cat. No.04CH37508)*, 284–289. doi:10.1109/CACSD.2004.1393890.

Lozano, R., Brogliato, B., Egeland, O., and Maschke, B. (2013). *Dissipative systems analysis and control: theory and applications*. Springer Science & Business Media.

Machado, J.E., Rinaldi, G., Cucuzzella, M., Menon, P.P., Scherpen, J.M., and Ferrara, A. (2023). Online parameters estimation schemes to enhance control performance in DC microgrids. *European Journal of Control*, 74, 100860.

Machado, J.E. and Schiffer, J. (2020). A passivity-inspired design of power-voltage droop controllers for DC microgrids with electrical network dynamics. In *2020 59th IEEE Conference on Decision and Control (CDC)*, 3060–3065. IEEE.

Malan, A.J., Ferguson, J., Cucuzzella, M., Scherpen, J.M., and Hohmann, S. (2025). Passivation of clustered DC microgrids with non-monotone loads. *IEEE Transactions on Control Systems Technology*.

Malan, A.J., Jané-Soneira, P., Strehle, F., and Hohmann, S. (2024). Passivity-based power sharing and voltage regulation in DC microgrids with unactuated buses. *IEEE Transactions on Control Systems Technology*, 32(4), 1410–1425. doi:10.1109/TCST.2024.3372308.

Markovsky, I. and Dörfler, F. (2021). Behavioral systems theory in data-driven analysis, signal processing, and control. *Annual Reviews in Control*, 52, 42–64.

Martinelli, A., Aboudonia, A., and Lygeros, J. (2024). Interconnection of (Q,S,R)-Dissipative Systems in Discrete Time. URL <https://arxiv.org/abs/2311.08088>.

Maupong, T., Mayo-Maldonado, J.C., and Rapisarda, P. (2017). On Lyapunov functions and data-driven dissipativity. *IFAC-PapersOnLine*, 50(1), 7783–7788.

Mei, W. and Bullo, F. (2017). LaSalle invariance principle for discrete-time dynamical systems: A concise and self-contained tutorial. *arXiv preprint arXiv:1710.03710*.

Moylan, P. and Hill, D. (1978). Stability criteria for large-scale systems. *IEEE Transactions on Automatic Control*, 23(2), 143–149. doi:10.1109/TAC.1978.1101721.

Nakano, T., Aboudonia, A., Eising, J., Martinelli, A., Dörfler, F., and Lygeros, J. (2025). Dissipativity-based data-driven decentralized control of interconnected systems. URL <https://arxiv.org/abs/2509.14047>.

Rosa, T.E. and Jayawardhana, B. (2021). On the one-shot data-driven verification of dissipativity of LTI systems with general quadratic supply rate function. In *2021 European Control Conference (ECC)*, 1291–1296. IEEE.

Schiffer, J., Aristidou, P., and Ortega, R. (2019). Online estimation of power system inertia using dynamic regressor extension and mixing. *IEEE Transactions on Power Systems*, 34(6), 4993–5001. doi:10.1109/TPWRS.2019.2915249.

Schiffer, J., Zonetti, D., Ortega, R., Stanković, A.M., Sezi, T., and Raisch, J. (2016). A survey on modeling of microgrids—from fundamental physics to phasors and voltage sources. *Automatica*, 74, 135–150. doi:<https://doi.org/10.1016/j.automatica.2016.07.036>.

Strehle, F., Machado, J.E., Cucuzzella, M., Malan, A.J., Hohmann, S., and Scherpen, J.M.A. (2024). A unifying passivity-based framework for pressure and volume flow rate control in district heating networks. *IEEE Transactions on Control Systems Technology*, 32(4), 1323–1340. doi: 10.1109/TCST.2024.3365250.

van Waarde, H.J., Camlibel, M.K., Rapisarda, P., and Trentelman, H.L. (2022). Data-driven dissipativity analysis: Application of the matrix s-lemma. *IEEE Control Systems Magazine*, 42(3), 140–149. doi:10.1109/MCS.2022.3157118.

van Waarde, H.J., Eising, J., Camlibel, M.K., and Trentelman, H.L. (2023). A behavioral approach to data-driven control with noisy input–output data. *IEEE Transactions on Automatic Control*, 69(2), 813–827.

Van Waarde, H.J., Eising, J., Camlibel, M.K., and Trentelman, H.L. (2023). The informativity approach: To data-driven analysis and control. *IEEE Control Systems Magazine*, 43(6), 32–66.

Verhoek, C., Berberich, J., Haesaert, S., Allgöwer, F., and Tóth, R. (2024). Data-driven dissipativity analysis of linear parameter-varying systems. *IEEE Transactions on Automatic Control*, 69(12), 8603–8616. doi: 10.1109/TAC.2024.3417855.

Weiland, S. and Cheng, X. (2022). Interconnection and approximation in networks of dissipative systems: Addressing topological simplification. *IEEE Control Systems Magazine*, 42(2), 107–117. doi:10.1109/MCS.2021.3139746.

Willems, J.C. (1972). Dissipative dynamical systems part i: General theory. *Archive for rational mechanics and analysis*, 45(5), 321–351.

Willems, J.C. (1986). From time series to linear system—part i. finite dimensional linear time invariant systems. *Automatica*, 22(5), 561–580. doi:[https://doi.org/10.1016/0005-1098\(86\)90066-X](https://doi.org/10.1016/0005-1098(86)90066-X).

Willems, J.C., Rapisarda, P., Markovsky, I., and De Moor, B.L. (2005). A note on persistency of excitation. *Systems & Control Letters*, 54(4), 325–329. doi: <https://doi.org/10.1016/j.sysconle.2004.09.003>.

Appendix A. MODELING SETUP

The (continuous-time) pre-contingency dynamics of each area is described by a model of the form of (17) plus a constant additive term d_i , and with the following coefficient matrices:

$$A_1 = \begin{bmatrix} -\frac{r_1}{l_1} & -\frac{1}{l_1}(1+k_{\text{prop},1}) & \frac{1}{l_1} & 0 \\ \frac{1}{c_1} & -\frac{1}{c_1 r_{\text{load},1}} & 0 & \frac{1}{c_1} \\ 0 & -k_{\text{integ},1} & 0 & 0 \\ 0 & -\frac{1}{L_{1,2}} & 0 & -\frac{r_{1,2}}{L_{1,2}} \end{bmatrix},$$

$$B_1 = \begin{bmatrix} 0 & 0 \\ \frac{1}{c_1} & 0 \\ 0 & 0 \\ 0 & \frac{1}{L_{1,2}} \end{bmatrix}, \quad C_1 = \begin{bmatrix} 0 & 1 & 0 & 0 \\ 0 & 0 & 0 & 1 \end{bmatrix},$$

$$d_1 = \begin{bmatrix} k_{\text{prop},1} x_{1,2}^* \\ l_1 \end{bmatrix} - \frac{i_{\text{load},1}}{c_1} \quad k_{\text{integ},1} x_{1,2}^* \quad 0 \quad \top,$$

and, for $i = 2, 3, 4$,

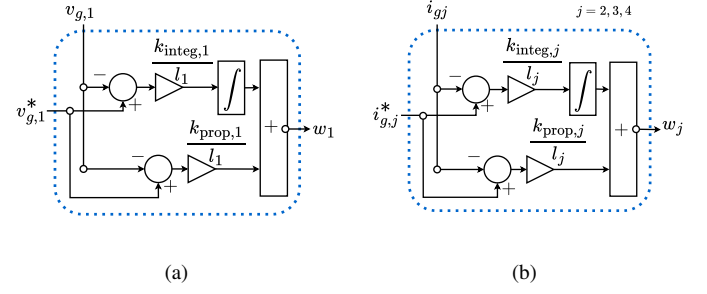


Fig. A.1. Controller setup (a) Voltage-setting PI controller for Area 1, (b) Current-setting PI controller for Areas 2,3 and 4.

Table A.1. Microgrid Parameters and Desired Set-points

Area	1	2	3	4
r_i (Ω)	0.2	0.3	0.5	0.1
l_i (mH)	1.8	2.0	3.0	2.2
c_i (mF)	2.2	1.9	2.5	1.7
$r_{\text{load},i}$ (Ω)	7.70	12.84	12.84	9.63
$i_{\text{load},i}$ (A)	16.45	9.87	9.87	13.16
$x_{1,2}^*$ (V)	380	–	–	–
$x_{i,1}^*$ (A)	–	39.47	39.47	52.63
k_{prop} (–)	2.1	19	35	1
k_{integ} (s^{-1})	60	11	14	1

Table A.2. Power Line Parameters

Line	{1,2}	{2,3}	{3,4}	{1,4}
$r_{i,j}$ (Ω)	0.70	0.60	0.80	0.90
$L_{i,j}$ (mH)	0.8	1	1	0.7

$$A_i = \begin{bmatrix} -\frac{1}{l_i}(r_i + k_{\text{prop},i}) & -\frac{1}{l_i} & \frac{1}{l_i} & 0 \\ \frac{1}{c_i} & -\frac{1}{c_i r_{\text{load},i}} & 0 & \frac{1}{c_i} \\ -k_{\text{integ},i} & 0 & 0 & 0 \\ 0 & -\frac{1}{L_{i,j}} & 0 & -\frac{r_{i,j}}{L_{i,j}} \end{bmatrix},$$

$$B_i = \begin{bmatrix} 0 & 0 \\ \frac{1}{c_i} & 0 \\ 0 & 0 \\ 0 & \frac{1}{L_{i,j}} \end{bmatrix}, \quad C_i = \begin{bmatrix} 0 & 1 & 0 & 0 \\ 0 & 0 & 0 & 1 \end{bmatrix},$$

$$d_i = \begin{bmatrix} k_{\text{prop},i} x_{i,1}^* \\ l_i \end{bmatrix} - \frac{i_{\text{load},i}}{c_i} \quad k_{\text{integ},i} x_{i,1}^* \quad 0 \quad \top.$$
(A.2)

The considered numerical parameters are shown in Tables A.1 and A.2. For each area, the components of the state vector $x_i = (x_{i,1}, x_{i,2}, x_{i,3}, x_{i,4})$ represent current generation $i_{g,i}$, bus voltage $v_{g,i}$, an integral control action $z_{g,i}$, and the current $i_{i,j}$ of one of the power lines incident to Area i : in Areas 1 to 4 we respectively embed the lines {1,2}, {2,3}, {3,4}, and {1,4}, with parameters $(r_{i,j}, L_{i,j})$; we set the convention that the reference direction for positive current $i_{i,j}$ is from j to i . The goal of the generation unit at Area 1 is to establish, through a PI-control action (see Fig. A.1), a desired steady-state bus voltage $x_{1,2}^*$, whereas the goal of the generation units at Areas 2, 3 and 4 is to establish (also through PI-control) desired steady-state current injections $x_{2,1}^*$, $x_{3,1}^*$ and $x_{4,1}^*$, respectively.